The nuclear receptor REV-ERBα is required for the daily balance of carbohydrate and lipid metabolism

Julien Delezie,* Stéphanie Dumont,* Hugues Dardente,[‡] Hugues Oudart,[†] Aline Gréchez-Cassiau,[§] Paul Klosen,* Michèle Teboul,[§] Franck Delaunay,[§] Paul Pévet,* and Etienne Challet*,[1]

*Department of Neurobiology of Rhythms, Institute of Cellular and Integrative Neurosciences, and [†]Department of Ecology, Physiology, and Ethology, Hubert Curien Multidisciplinary Institute, University of Strasbourg, Strasbourg, France; [‡]Physiology of Reproduction and Behavior, François Rabelais University, French Institute of the Horse and Equitation, Nouzilly, France; and [§]Valrose Institute of Biology, University of Nice, Nice, France

ABSTRACT   Mutations of clock genes can lead to diabetes and obesity. REV-ERBα, a nuclear receptor involved in the circadian clockwork, has been shown to control lipid metabolism. To gain insight into the role of REV-ERBα in energy homeostasis *in vivo*, we explored daily metabolism of carbohydrates and lipids in chow-fed, unfed, or high-fat-fed *Rev-erbα*^{−/−} mice and their wild-type littermates. Chow-fed *Rev-erbα*^{−/−} mice displayed increased adiposity (2.5-fold) and mild hyperglycemia (~10%) without insulin resistance. Indirect calorimetry indicates that chow-fed *Rev-erbα*^{−/−} mice utilize more fatty acids during daytime. A 24-h nonfeeding period in *Rev-erbα*^{−/−} animals favors further fatty acid mobilization at the expense of glycogen utilization and gluconeogenesis, without triggering hypoglycemia and hypothermia. High-fat feeding in *Rev-erbα*^{−/−} mice amplified metabolic disturbances, including expression of lipogenic factors. *Lipoprotein lipase* (*Lpl*) gene, critical in lipid utilization/storage, is triggered in liver at night and constitutively up-regulated (~2-fold) in muscle and adipose tissue of *Rev-erbα*^{−/−} mice. We show that CLOCK, up-regulated (2-fold) at night in *Rev-erbα*^{−/−} mice, can transactivate *Lpl*. Thus, overexpression of *Lpl* facilitates muscle fatty acid utilization and contributes to fat overload. This study demonstrates the importance of clock-driven *Lpl* expression in energy balance and highlights circadian disruption as a potential cause for the metabolic syndrome.—Delezie, J., Dumont, S., Dardente, H., Oudart, H., Gréchez-Cassiau, A., Klosen, P., Teboul, M., Delaunay, F., Pévet, P., Challet, E. The nuclear receptor REV-ERBα is required for the daily balance of carbohydrate and lipid metabolism. *FASEB J.* 26, 3321–3335 (2012). www.fasebj.org

Key Words: circadian · obesity · hyperglycemia · respiratory quotient · lipoprotein lipase

ALTERED CIRCADIAN RHYTHMICITY is a newly identified determinant of metabolic disorders in humans (1). Most aspects of behavior and metabolism display daily rhythms, including sleep-wake and feeding-nonfeeding cycles (2). These daily variations are controlled by a circadian timing system made of interconnected clocks and oscillators. In mammals, the master circadian clock, located in the suprachiasmatic nuclei of the hypothalamus, is mainly reset by ambient light and synchronizes peripheral oscillations to 24 h. Secondary oscillators are present in many brain regions and peripheral organs (*e.g.*, liver), and can be shifted by feeding-related cues (3–5).

The molecular clockwork is based on autoregulatory transcriptional and translational feedback loops involving clock genes and proteins that generate a rhythmic transcriptional activity with a ~24 h period. In this clock network, two transcriptional activators, CLOCK and BMAL1, stimulate the expression of *Period* (*Per1–3*) and *Cryptochrome* (*Cry1, 2*) genes, whose proteins in turn repress the CLOCK-BMAL1 transactivation (6). In addition to these main components, the nuclear receptors ROR(α,β,γ) and REV-ERB(α,β) compete to activate and repress, respectively, the transcription of the *Bmal1* and *Clock* genes, thereby reinforcing the robustness of circadian oscillations (7–9).

Approximately 10% of the mammalian transcriptome is under circadian regulation (10). In particular,

---

Abbreviations: AUC, area under the curve; DMEM, Dulbecco's modified Eagle's medium; GST, glucagon stimulation test; HDL, high-density lipoprotein; HFD, high-fat diet; IPIST, intraperitoneal insulin sensitivity test; LDL, low-density lipoprotein; MyHC, myosin heavy chain; NEFA, nonesterified fatty acid; OGTT, oral glucose tolerance test; PTT, pyruvate tolerance test; RLU, relative luminescence unit; RQ, respiratory quotient; VLDL, very low density lipoprotein; WAT, white adipose tissue; ZT, zeitgeber time

metabolic processes are closely linked to circadian oscillations, as evidenced by the transcriptional control of genes involved in lipid and glucose metabolism by clock-related factors (3, 11). Consequently, disruption of the circadian clockwork leads to profound changes in energy balance. Mutation of *Clock* leads to obesity (12), while pancreas-specific *Bmal1*-mutant mice develop diabetes (13). On the other hand, diet-induced obesity affects the master clock as well as peripheral oscillations in wild-type mice (14, 15) and exacerbates metabolic phenotypes in mice with deficient clocks (12, 16).

As outlined above, REV-ERBα is a component of the circadian clockwork that is expressed in the brain and peripheral tissues, such as liver, pancreas, adipose tissue, and muscle (8, 17, 18). Furthermore, REV-ERBα participates in the regulation of diverse metabolic pathways, including adipocyte differentiation, gluconeogenesis, bile acid synthesis, and cholesterol homeostasis (19–22). Besides, REV-ERBα can modulate the expression of its own ligand, heme (23, 24), implicated in cellular metabolism. Daily expression of REV-ERBα has also been shown to control the circadian transcription of various lipid metabolism genes by recruiting the repressive chromatin modifier histone deacetylase 3 in the liver (25). Taken together, these data suggest that REV-ERBα may tightly connect the circadian system to energy metabolism on a daily basis.

Here we show that mice lacking *Rev-erbα* display changes in daily energy homeostasis, leading to enhanced lipid fuel utilization and production during daytime and nighttime, respectively, and predisposing to diet-induced obesity. This occurs with constitutive elevation of the *Lpl* gene in peripheral tissues, likely due to the defective clock regulation of this gene.

MATERIALS AND METHODS

Animals and housing conditions

Rev-erbα$^{+/-}$ mice, kindly provided by Prof. Ueli Schibler (University of Geneva, Geneva, Switzerland) were rederived on a C57BL6/J background (Charles River Laboratories, L'Arbresle, France) and backcrossed until N5 in our local animal care facilities (Chronobiotron, Strasbourg, France). Characterization of the genetic background of the strain by Charles River Laboratories indicated that mice were >95% C57BL6/J. The *Rev-erbα*-deletion strategy is described in ref. 8. All mice were maintained under a 12-h light-dark cycle in a temperature-controlled room (22 ± 1°C). Normocaloric chow diet (2.89 kcal/g, 14% kcal from fat, 27% kcal from protein and 59% from carbohydrates; SAFE 105; SAFE, Augy, France) and water were provided *ad libitum* unless specified otherwise. All experiments were performed in accordance with the U.S. National Institutes of Health Guide for the Care and Use of Laboratory Animals (1996), the French National Law (implementing the European Communities Council Directive 86/609/EEC) and approved by the Regional Ethical Committee of Strasbourg for Animal Experimentation (CREMEAS).

Animal experiments

Behavior, physiology, and glucose homeostasis

Mice (4 mo old, *n*=10/genotype, sex ratio 1:1) were used for measuring general locomotor activity and body temperature after intraperitoneal implantation with a small transponder (G2 E-Mitter; MiniMitter, Sunriver, OR, USA) under gaseous anesthesia (2% isoflurane in 50:50 O$_2$/N$_2$O). Locomotor activity and temperature data were recorded every 5 min, 24 h/d, with a PC-based acquisition system (VitalView; Mini-Mitter) and analyzed with Clocklab (Actimetrics, Evanston, IL, USA). Indirect calorimetry was performed on other mice (*n*=10/genotype, sex ratio 1:1) as described previously (26) as well as the hepatocyte study (see procedure below). For glucose, insulin measurements and pancreas studies, mice (*n*=12/genotype, sex ratio 1:1) were sampled at zeitgeber time 0 (ZT0; lights on, onset of the resting/nonfeeding period) and ZT12 (lights off, onset of the active/feeding period).

Food withdrawal and refeeding experiments

Mice (4 mo old) were divided into 2 groups (4 males and 3 females/group/genotype); one group was unfed for 24 h starting at ZT0, and the other was unfed for 24 h and then refed for the next 24 h with a high-carbohydrate diet (3.63 kcal/g, 7.4% kcal from fat, 14.1% kcal from protein, and 78.5% kcal from carbohydrate; SAFE U8960v2). Both groups were killed by lethal injection of pentobarbital at ZT0. Blood samples were collected with 4% EDTA and centrifuged for 10 min at 5000 rpm at 4°C. Liver samples were flash-frozen in liquid nitrogen. Locomotor activity and body temperature were recorded as above.

High-fat-diet (HFD) challenge

Mice (4 wk old, sex ratio 1:1) were fed either with a chow diet (as described above; *n*=12/genotype) or an HFD (4.65 kcal/g, 53.2% kcal from fat, 14.6% kcal from protein and 32.2% kcal from carbohydrate, SAFE U8955v3; *n* = 12/genotype) for up to 12 wk. Then, animals were sacrificed at ZT0 and ZT12. Mice were unfed for 1 h before injection of a lethal dose of pentobarbital. Blood samples were collected as above. Liver, white adipose tissue (WAT; retroperitoneal and perigonadal), and rectus femoris muscle were taken and immediately flash-frozen in liquid nitrogen.

In vivo glucose homeostasis

The blood glucose rhythm was determined in mice fed *ad libitum* from repeated tail-blood microsamples (<0.5 μl) using an Accu-Check glucometer (Roche Diagnostics, Meylan, France). For all metabolic tests, mice were unfed for 14 h (from ZT12 to ZT2) and injected at ZT2. For the oral glucose tolerance test (OGTT), mice received a glucose load *via* gavage (2 g/kg; D-glucose; Sigma, Saint Quentin Fallavier, France). For the glucagon stimulation test (GST) and pyruvate tolerance test (PTT), glucagon (1 mg/kg; GlucaGen; Novo Nordisk, Bagsvaerd, Denmark) and pyruvate (1.5 g/kg; P5280; Sigma) were administered intraperitoneally. Note that metabolic tests were separated by several days. The euglycemic clamp study was done by the Mouse Clinical Institute (MCI; Strasbourg, France) from ZT6 in animals previously unfed from ZT0 to ZT6 (see method in ref. 27).

Pancreatic histology and immunohistochemistry

Pancreases were fixed in Bouin's solution for 24 h and dehydrated successively in 70% ethanol, 2-ethoxyethanol, and

butanol. The tissue was embedded in paraffin, and 8-μm-thick serial sections were cut on a microtome and collected on gelatin-coated slides. For determination of islet area and circularity, sections were stained with Carrazzi's hematoxylin. To assess insulin and glucagon content, sections were washed with Tris buffered saline and incubated overnight with either mouse anti-insulin (1:50,000; clone HUI018; Novo Nordisk) or mouse anti-glucagon (1:60,000; clone GlU001; Novo Nordisk) antibodies. The sections were then rinsed and incubated for 1 h with a biotinylated secondary antibody (1:2000; Jackson ImmunoResearch, West Grove, PA, USA). Finally, streptavidin-peroxidase conjugate (1:2000; Roche) was added for 1 h after washing. Peroxidase activity was visualized with 0.5 mg/ml 3,3′-diaminobenzidine (Sigma) in the presence of 0.003% H_2O_2 in 50 mM Tris buffer containing 10 mM imidazole (pH 7.6). Micrographs were taken on a Leica DMRB microscope (Leica Microsystems, Nanterre, France) with an Olympus DP50 digital camera (Olympus, Rungis, France) and analyzed with ImageJ software (W. S. Rasband, U. S. National Institutes of Health, Bethesda MD, USA).

Plasma metabolic parameters

Total, low-density lipoprotein (LDL), and high-density lipoprotein (HDL) cholesterol levels were determined by a direct colorimetric method (Biolabo, Maizy, France). Plasma leptin was assayed with an ELISA kit (Leptin EZML-82K; Millipore, Molsheim, France). Plasma glucose was evaluated with a GOD-PAP kit (Biolabo). Plasma insulin was determined with an ultrasensitive mouse insulin ELISA kit (Crystal Chem, Downers Grove, IL, USA). Plasma glucagon was assayed with a glucagon RIA (GL-32K, Millipore) after adding aprotinin (250 kIU/ml) when blood samples were taken. Triglyceride concentration was determined by a triglyceride determination kit (TR-0100; Sigma). The ACS-ACOD method (NEFA-HR2; Wako, Osaka, Japan) was used for assaying plasma nonesterified fatty acids (NEFAs). Plasma β-hydroxybutyrate concentrations were determined with a cyclic enzymatic method (Autokit 3-HB; Wako).

Hepatic glycogen and triglycerides

Hepatic glycogen and triglycerides were assayed following the methods of Murat and Serfaty (28) and Miao *et al.* (29), respectively.

Primary hepatocyte culture

Livers sampled from adult mice at ZT2 to ZT4 were immediately perfused at the flow rate of 3 ml/min *via* the portal vein for 5 min with a calcium-free perfusion buffer (10 mM HEPES, 140 mM NaCl, and 6.7 mM KCl, pH 7.65), supplemented by 0.6 mM EGTA, followed by an additional 2 min with the Ca^{2+}-free buffer, then 5 min with the same buffer containing 5 mM $CaCl_2$ and 15 mg/ml thermolysin (Liberase, medium research grade; Roche). All solutions were kept at 37°C. The livers were then excised, and hepatocytes were released by mechanical disruption of the liver capsule into 20 ml of Leibovitz L-15 medium (Invitrogen, Cergy-Pontoise, France) supplemented with 100 IU penicillin and 100 mg/ml streptomycin. The cells were filtered through a 70-μm nylon mesh and centrifuged at 800 rpm for 2 min. The supernatant and cell debris were aspirated, and the cell pellet was washed 2 times into 10 ml of the same medium. The resulting cell pellet was finally resuspended in William's medium E with Glutamax (Invitrogen) containing 10% fetal bovine serum (Invitrogen), 100 IU penicillin, 100 mg/ml streptomycin, and 0.2 μM insulin. Hepatocyte viability was assessed by trypan blue exclusion. Hepatocytes were placed at 2.5×10^4 cells/cm^2 in collagen-coated 35-mm plates and cultured for up to 6 h in the resuspended medium at 37°C in 5% CO_2 chamber. After cell attachment, the medium was renewed without fetal calf serum and supplemented with 10 nM dexamethasone and 20 nM insulin for 12–16 h. Glucose production was measured 2 and 24 h after incubation of hepatocytes in glucose-free Dulbecco's modified Eagle's medium (DMEM) supplemented with 16 mM lactate, 4 mM pyruvate, 10 nM dexamethasone, and 20 nM insulin. Glucose release in the medium was determined by the GOD-POD colorimetric method (Sclavo Diagnostics International, Soviclle, Italy) and normalized to the protein concentration determined by the Bradford method.

mRNA extraction and quantitative real-time PCR

Samples of frozen livers were homogenized in lysis buffer supplemented with β-mercaptoethanol, and total RNA was extracted (Absolutely RNA Miniprep Kit; Stratagene; Agilent Technologies, Santa Clara, CA, USA) according to the manufacturer's protocol. The RNA samples were further purified by precipitation with sodium acetate and isopropyl alcohol. For retroperitoneal WAT and rectus femoris muscle samples, homogenization was done with QIAzol Lysis Reagent (Qiagen, Courtaboeuf, France), and total RNA was extracted using an RNeasy Lipid Tissue Mini Kit (Qiagen) according to the manufacturer's protocol. RNA quality was evaluated with the Bioanalyzer 2100 (Agilent Technologies; RNA integrity number for all samples was >7). RNA quantity was measured using a NanoDrop ND-1000 spectrophotometer (NanoDrop Technologies, Wilmington, DE, USA; A_{260}/A_{280} and A_{260}/A_{230} values were >1.8). cDNAs were synthesized from 1 μg of total RNA using the High Capacity RNA-to-cDNA Kit (Applied Biosystems, Courtaboeuf, France). Quantitative Real-time PCR was performed and analyzed using a 7300 Real-Time PCR System with 1× SYBR Green PCR Master Mix (Applied Biosystems), 0.9 μM primers (Invitrogen), and 1 μl of cDNA in a total volume of 20 μl. PCR conditions were 10 min at 95°C, followed by 40 cycles of 15 s at 95°C and 1 min at 60°C. PCR reactions were done in duplicate and negative controls (*i.e.*, no reverse transcription and no template controls) were added to the reactions. Relative expression levels were determined using the comparative ΔC_T method to normalize target gene mRNA to *36b4*. Primers were designed and optimized for an annealing temperature of 60°C. To assess primer specificity and product uniformity, sequences were tested with the Basic Local Alignment Search Tool (BLAST; U.S. National Center for Biotechnology Information; http://blast.ncbi.nlm.nih.gov/), and postamplification dissociation curves were determined. A dilution curve of the pool of all cDNA samples was used to calculate the amplification efficiency for each assay (values were between 1.85 and 2). Primer sequences are summarized in Supplemental Table S1.

Cell culture, transfection, and luciferase assay

COS-7 cells were grown in DMEM supplemented with 10% fetal bovine serum (Life Technologies, Inc.; Invitrogen), 1% penicillin/streptomycin (Life Technologies) mix and sodium pyruvate in a humidified atmosphere with 5% CO_2 at 37°C. Cells were plated in 24-well plates and transfected with GeneJuice (Novagen; Merck, Darmstadt, Germany). Depending on the experiment, hRORα and hREV-ERBα expression vectors (7) were used at either 100 or 200 and 200 ng/well, respectively. The o*Bmal1-luc* and *mPer1-luc* reporter construct and m*Clock*/m*Bmal1* expression vectors have been used pre-

viously (30,31). The proximal promoter region of m*Lpl* (−143 to +186) was cloned in pGL3 basic (see Supplemental Data for further information). All reporter constructs and β-galactosidase reporter construct were used at 50 and 100 ng/well, respectively. Total transfected DNA amount was set to an equal amount between all conditions by addition of the corresponding empty vector. Luciferase assay was performed 48 h after transfection. Briefly, cells were rinsed twice in cold PBS and lysed for 15 min in lysis buffer (25 mM Tris, 2 mM EDTA, 1 mM dithiothreitol, 10% glycerol, and 1% TritonX-100). The luciferase assay was performed using a luciferase assay system kit (Promega, Charbonnieres, France) and a PolarStar Optima luminometer (BMG Labtech, Ortenberg, Germany). Results were normalized to β-galactosidase activity. Data [in relative luminescence units (RLU)] represent fold induction once normalized to β-galactosidase. Experiments were repeated 3 times, each condition in triplicate.

Statistical analysis

All values are presented as means ± SE. Area under the curve (AUC) was determined as incremental area (*i.e.*, above baseline; see ref. 27). The 48-h respiratory quotient (RQ) data were fitted to a cosinor function [$f = a + (b * \cos (2 * \pi * (x - c)/24))$], where x indicates the time, a the mean value, b the amplitude, and c the acrophase. Statistical difference between genotypes for a given parameter (*e.g.*, amplitude) was tested in an analysis of covariance. Normality and homogeneity of variance were assessed with Kolmogorov-Smirnov and Lilliefors test and Levene's test, respectively. Data that were non-normal and/or heteroscedastic were subjected to logarithmic transformation before analysis. Value of α was set at 0.05. Unpaired Student's *t* test was used to compare 2 groups. Luciferase assay data were analyzed using 1-way analyses of variance (ANOVA) followed by Tukey HSD *post hoc* analysis. Data collected successively at different time points (*e.g.*, locomotor activity) within each group were compared with ANOVA for repeated measures. Two-way ANOVA was performed to assess the effects of genotype and feeding condition and the interaction between these factors. Three-way ANOVA design was employed to test the aforementioned

factors plus the effect of time. Simple main effects approach was conducted to examine each factor separately if the interaction term was significant. Statistical analyses were performed with Statistica 10 (StatSoft, Maisons-Alfort, France).

RESULTS

Rev-erbα$^{-/-}$ mice are slightly hyperglycemic without insulin resistance

We first evaluated whether *Rev-erbα* deficiency affects general physiology and behavior. No significant difference was found between *Rev-erbα*$^{-/-}$ mice and their wild-type (+/+) littermates regarding the amount and timing of chow intake (**Fig. 1A**). Body mass was not significantly different between 4-mo-old *Rev-erbα*$^{+/+}$ and *Rev-erbα*$^{-/-}$ mice (24.02 ± 1.11 *vs.* 25.58 ± 1.20 g, respectively). The daily patterns of general locomotor activity and body temperature were very close in the two genotypes (Fig. 1*B*, *C*). In sharp contrast, 24-h blood glucose rhythm showed higher values in *Rev-erbα*$^{-/-}$ mice compared to *Rev-erbα*$^{+/+}$ mice (Fig. 1*D*), suggesting altered glucose homeostasis. Of note, mild hyperglycemia at the day-night transition has been previously observed in *Rev-erbα*$^{-/-}$ mice (20). To understand the origin of this hyperglycemia in *Rev-erbα*$^{-/-}$ mice, we determined the day-night levels of insulin, glucagon, and hepatic glycogen in both genotypes. Plasma insulin was increased at ZT0 (lights on, onset of the resting period; **Fig. 2A**), while hepatic glycogen content was higher at ZT12 (lights off, onset of the active period; Fig. 2*B*). These higher insulin and glycogen levels in *Rev-erbα*$^{-/-}$ mice are consistent with previous results (20, 32). Plasma glucagon levels showed no difference between genotypes (Fig. 2*C*). According to standardized guidelines (27), we then compared the responses
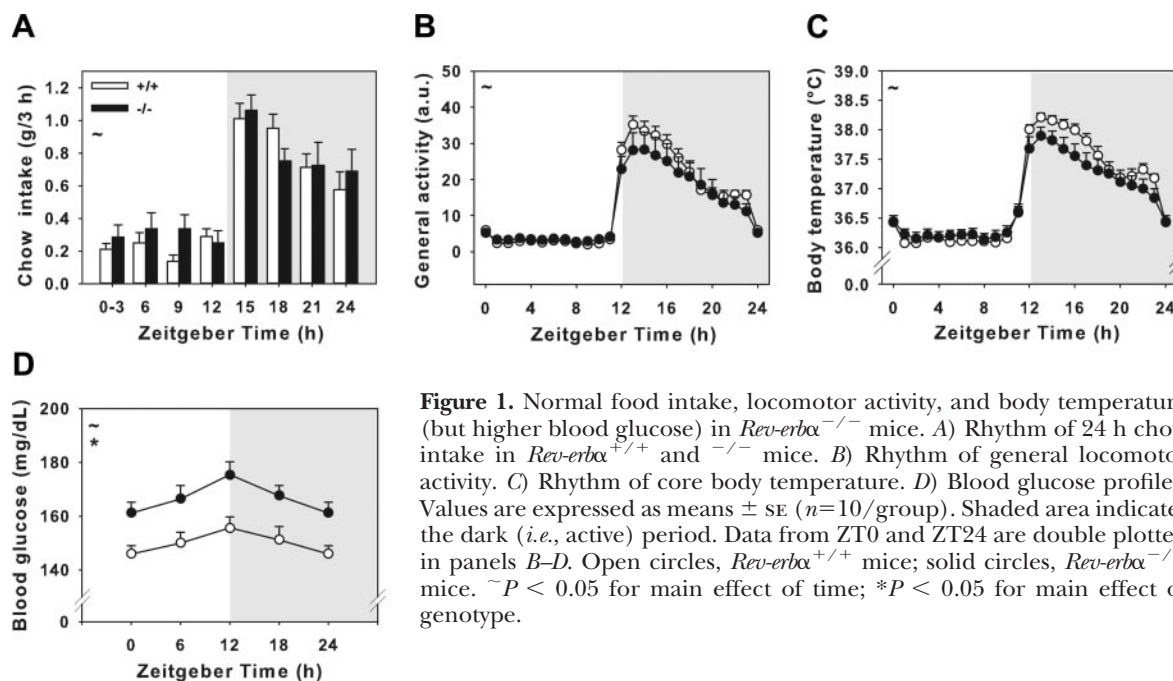

Figure 1. Normal food intake, locomotor activity, and body temperature (but higher blood glucose) in *Rev-erbα*$^{-/-}$ mice. *A*) Rhythm of 24 h chow intake in *Rev-erbα*$^{+/+}$ and $^{-/-}$ mice. *B*) Rhythm of general locomotor activity. *C*) Rhythm of core body temperature. *D*) Blood glucose profiles. Values are expressed as means ± SE (*n*=10/group). Shaded area indicates the dark (*i.e.*, active) period. Data from ZT0 and ZT24 are double plotted in panels *B–D*. Open circles, *Rev-erbα*$^{+/+}$ mice; solid circles, *Rev-erbα*$^{-/-}$ mice. $^{\sim}P < 0.05$ for main effect of time; $*P < 0.05$ for main effect of genotype.
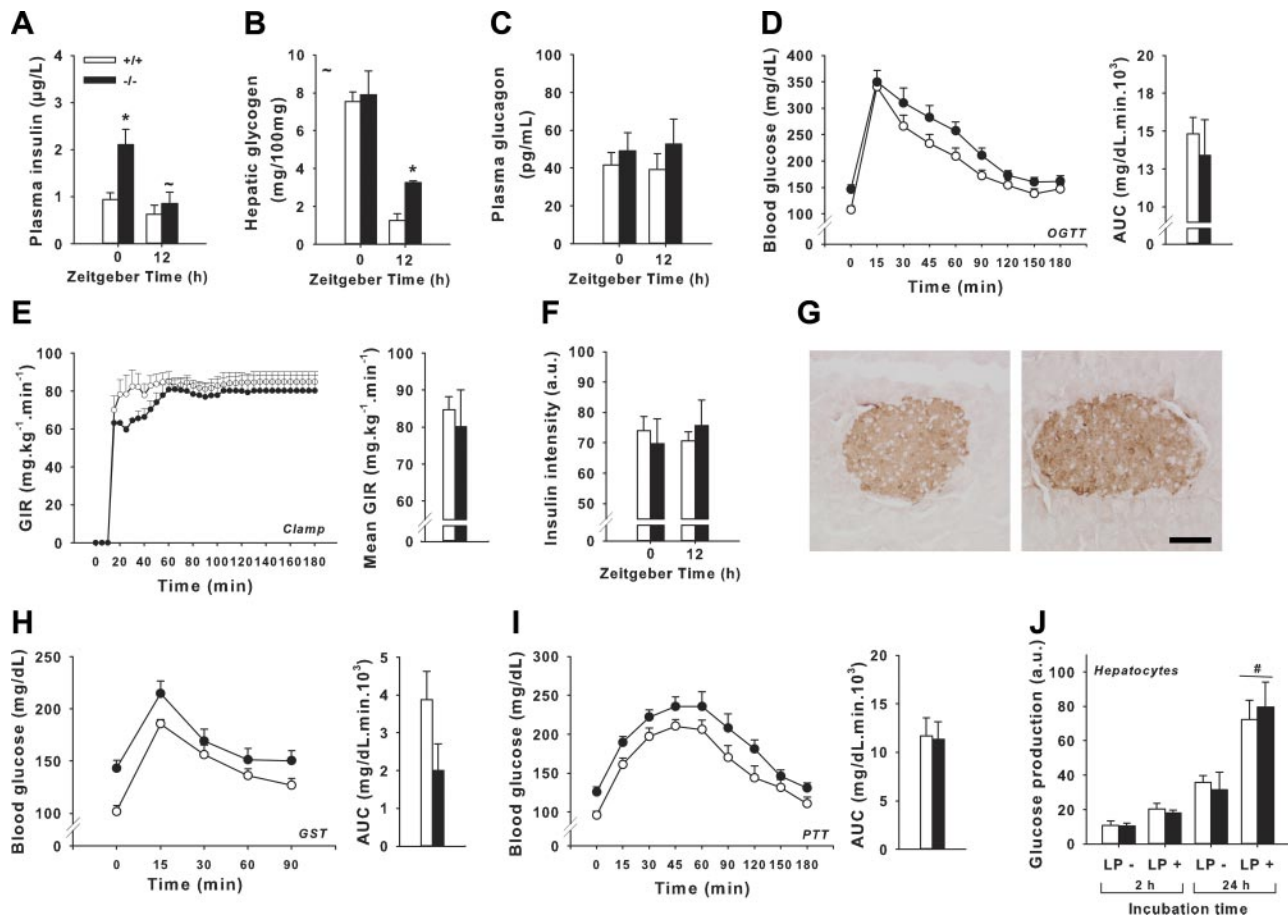
Figure 2. Lack of whole insulin resistance or increased gluconeogenesis in *Rev-erbα*$^{-/-}$ mice. *A–C*) Plasma insulin levels (*A*), hepatic glycogen concentration (*B*), and plasma glucagon levels (*C*); $n = 6$/group. *D*) OGTT in mice unfed overnight (*i.e.*, from ZT12 to ZT2) and the resulting incremental AUC ($n=12$/group). *E*) Hyperinsulinemic-euglycemic clamp and the resulting glucose infusion rates averaged over the last 60 min of the clamp ($n=6$/group). *F*) Insulin immunostaining from pancreas sections of $+/+$ and $-/-$ animals and their respective quantification ($n=6$/group). *G*) Pancreas sections of a *Rev-erbα*$^{+/+}$ (left panel) and a *Rev-erbα*$^{-/-}$ mouse (right panel) stained with insulin antibody. Scale bar = 50 μm. *H, I*) GST (*H*) and PTT (*I*) in mice unfed overnight and the resulting AUCs ($n=12$/group). *J*) Glucose production in *Rev-erbα*$^{+/+}$ and *Rev-erbα*$^{-/-}$ primary hepatocytes incubated with ($+$) or without ($-$) lactate-pyruvate (LP) for 2 or 24 h ($n=7$/group). Data are means ± se. Open circles, *Rev-erbα*$^{+/+}$ mice; solid circles, *Rev-erbα*$^{-/-}$ mice. ~$P < 0.05$ for main effect of time (top left corner) or *vs.* corresponding ZT0 group of same genotype (above bar); *$P < 0.05$ *vs.* $+/+$ genotype at same ZT; #$P < 0.05$ *vs.* 24 h LP$-$ treatment.

of both genotypes to metabolic challenges, by comparing their respective AUC values, calculated as incremental area (above baseline, to exclude the effect of differences in fasting glucose levels between animals). The OGTT (performed at the same ZTs as in ref. 13) showed no significant difference between genotypes either at ZT2 (Fig. 2*D*) or at ZT14 (Supplemental Fig. S1*C*). Insulin sensitivity, assessed by the intraperitoneal insulin sensitivity test (IPIST), was not significantly modified in *Rev-erbα*$^{-/-}$ mice compared to wild-type mice, either at ZT2 (despite a trend toward increased sensitivity; $P=0.07$ for AUC; Supplemental Fig. S1*B*), or at ZT14 (Supplemental Fig. S1*D*). When *Rev-erbα*$^{-/-}$ mice were challenged with an OGTT after overnight food withdrawal, their glucose-stimulated insulin secretion was also similar to that of control mice (Supplemental Fig. S1*A*). Similarly, a hyperinsulinemic-euglycemic clamp study performed from ZT6 in animals previously unfed for 6 h indicated that the glucose infusion rate, averaged over the last 60 min of the

clamp, was similar between genotypes (Fig. 2*E*), ruling out any major alteration in whole-body insulin sensitivity. In addition, pancreatic islets from both genotypes were identical in area, circularity, and insulin content (Fig. 2*F, G* and Supplemental Fig. S2*A*). Altogether, these observations suggest that the high blood glucose seen in chow-fed *Rev-erbα*$^{-/-}$ mice is not the result of either insulin resistance or a defect in insulin secretion.

Gluconeogenesis is not enhanced in *Rev-erbα*$^{-/-}$ mice

The following experiments were conducted to determine whether the hyperglycemia in *Rev-erbα*$^{-/-}$ mice was of hepatic origin. For that purpose, we investigated glycogenolysis by challenging mice with a GST. *Rev-erbα*$^{-/-}$ mice did not show a larger hyperglycemic response compared to that in controls (Fig. 2*H*), excluding hypersensitivity to glucagon as a potential cause of hyperglycemia. We then challenged mice with a PTT at ZT2 to investigate a potentially greater contribution

of gluconeogenesis in $Rev\text{-}erb\alpha^{-/-}$ mice. No significant difference was detected between the genotypes (Fig. 2*I*). Metformin, known to decrease hepatic glucose production by inhibiting gluconeogenesis and increasing insulin sensitivity, improved glucose tolerance to the same degree in both genotypes (data not shown). To confirm these *in vivo* results, we compared glucose production *in vitro* in primary hepatocytes from $Rev\text{-}erb\alpha^{-/-}$ and control animals. Following 24 h incubation in the presence of lactate-pyruvate, $Rev\text{-}erb\alpha^{-/-}$ hepatocytes did not produce more glucose than wild-type cells (Fig. 2*J*). We conclude that the chronic hyperglycemic phenotype of $Rev\text{-}erb\alpha^{-/-}$ mice cannot be explained by increased gluconeogenesis. As REV-ERBα is a potential link between the circadian timing system and metabolism, we hypothesized that these mice may exhibit a circadian misalignment of energy utilization.

Daily balance in energy stores utilization is exacerbated in $Rev\text{-}erb\alpha^{-/-}$ mice

To test whether the daily cycle of lipid and glucose utilization is modified in $Rev\text{-}erb\alpha^{-/-}$ mice, we assessed the 24-h variations of energy metabolism *in vivo* by using indirect calorimetry. Basal metabolism, determined from the 5 lowest O_2 consumption values during the second 24-h cycle, was not significantly different between genotypes (Supplemental Fig. S3). The RQ (V_{CO_2}/V_{O_2}) tracks the type of fuel oxidized. High (*i.e.*, close to 1) and low (*i.e.*, close to 0.7) RQ values indicate preferential utilization of carbohydrates and lipids, respectively. Of interest, $Rev\text{-}erb\alpha^{-/-}$ mice showed altered daily variations in RQ values compared to control mice, with lower and higher values during the day and the night, respectively (**Fig. 3*A, B***). Cosinor fitting followed by analysis of covariance of 48 h RQ data revealed that the acrophase of RQ occurred 1.4 h later (*i.e.*, was phase delayed) in $Rev\text{-}erb\alpha^{-/-}$ compared to control mice (ZT 17.4 ± 0.1 *vs.* 16.0 ± 0.2, respectively; $P < 0.001$). Furthermore, daily changes of RQ in $Rev\text{-}erb\alpha^{-/-}$ mice displayed larger amplitude than in control littermates (0.11 ± 0.003 *vs.* 0.06 ± 0.003, respectively; $P < 0.001$), whereas the daily mean RQ, which reflects energy homeostasis, did not differ between genotypes (+/+ *vs.* −/−: 0.85 ± 0.002 *vs.* 0.85 ± 0.002, respectively).

These data demonstrate that $Rev\text{-}erb\alpha^{-/-}$ mice have increased fatty acid utilization during the resting period compared to littermate controls, while their glucose utilization (*i.e.*, glucose supply to active organs and/or conversion of dietary carbohydrates to fat) is delayed and increased during the active period.

Increased utilization of lipid fuels in unfed $Rev\text{-}erb\alpha^{-/-}$ mice

To test a preferential use of fatty acids over glucose in $Rev\text{-}erb\alpha^{-/-}$ mice, we analyzed the physiological and hepatic molecular responses of both genotypes after 24 h of food withdrawal (*i.e.*, to trigger mobilization of energy stores) and 24 h of food withdrawal followed by 24 h refeeding with high-carbohydrate diet (*i.e.*, to trigger lipogenesis). Changes in body mass associated with food withdrawal and refeeding did not differ significantly between the genotypes (**Fig. 4*A***). Compared to controls, $Rev\text{-}erb\alpha^{-/-}$ mice exhibited a significantly lower hypothermia response to 24 h of food deprivation, resulting in higher body temperature at the end of the nonfeeding period (Fig. 4*B*). This lack of hypothermia was not due to changes in the level of locomotor activity (Supplemental Fig. S4*A*). In addition, fasting blood glucose levels were still significantly higher in $Rev\text{-}erb\alpha^{-/-}$ mice compared to $Rev\text{-}erb\alpha^{+/+}$ animals (Fig. 4*C*). This confirms the mild hyperglycemia after overnight food withdrawal before metabolic tests. However, there was no difference between the genotypes in the refeeding condition (Fig. 4*C*). The absence of hyperglycemia in refed $Rev\text{-}erb\alpha^{-/-}$ mice was not linked to differential changes in insulin levels (Fig. 4*D*) or food intake (+/+ *vs.* −/−: 6.09 ± 0.16 *vs.* 6.33 ± 0.17 g, respectively). One possible explanation is that previously unfed $Rev\text{-}erb\alpha^{+/+}$ mice are more sensitive than $Rev\text{-}erb\alpha^{-/-}$ animals to the hyperglycemic effect of high-carbohydrate diet. In other words, $Rev\text{-}erb\alpha^{-/-}$ mice may be more efficient to process high-carbohydrate intake for fatty acid synthesis.

While most metabolic parameters studied did not differ between the two genotypes in the refed condition (Fig. 4*D–I*), many of them were differentially affected by 24 h of food withdrawal in $Rev\text{-}erb\alpha^{+/+}$ *vs.* −/− animals. In particular, hepatic glycogen was significantly more elevated in $Rev\text{-}erb\alpha^{-/-}$ mice (Fig. 4*E*), indicating that blood glucose is not used as a primary source of energy in these mice. Interestingly, plasma

Figure 3. Changes in daily fuel utilization in $Rev\text{-}erb\alpha^{-/-}$ mice. *A*) RQ (48 h; *i.e.*, V_{CO_2}/V_{O_2} values) of $Rev\text{-}erb\alpha^{+/+}$ and $^{-/-}$ mice, determined by indirect calorimetry. Shaded and solid traces show fitting of the 48-h RQ data of $Rev\text{-}erb\alpha^{+/+}$ and $Rev\text{-}erb\alpha^{-/-}$ mice, respectively, to the cosine function. Note that data were collected every 15 min. Shaded area indicates the dark (*i.e.*, active/feeding) period. Open circles, $Rev\text{-}erb\alpha^{+/+}$ mice; solid circles, $Rev\text{-}erb\alpha^{-/-}$ mice. *B*) Day and night averages of RQ. Values are expressed as means ± SE (n=10/group). ~$P < 0.05$ for main effect of time.
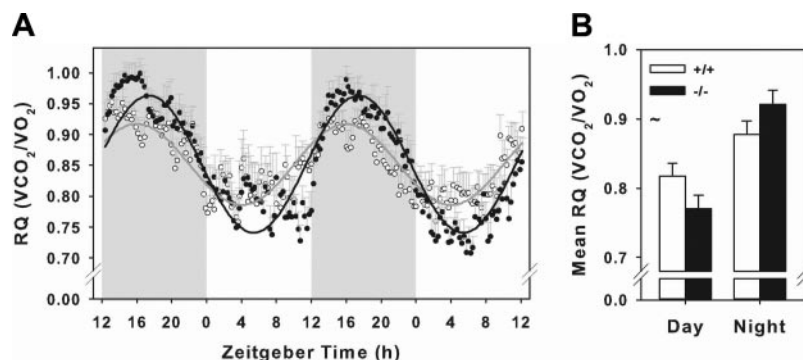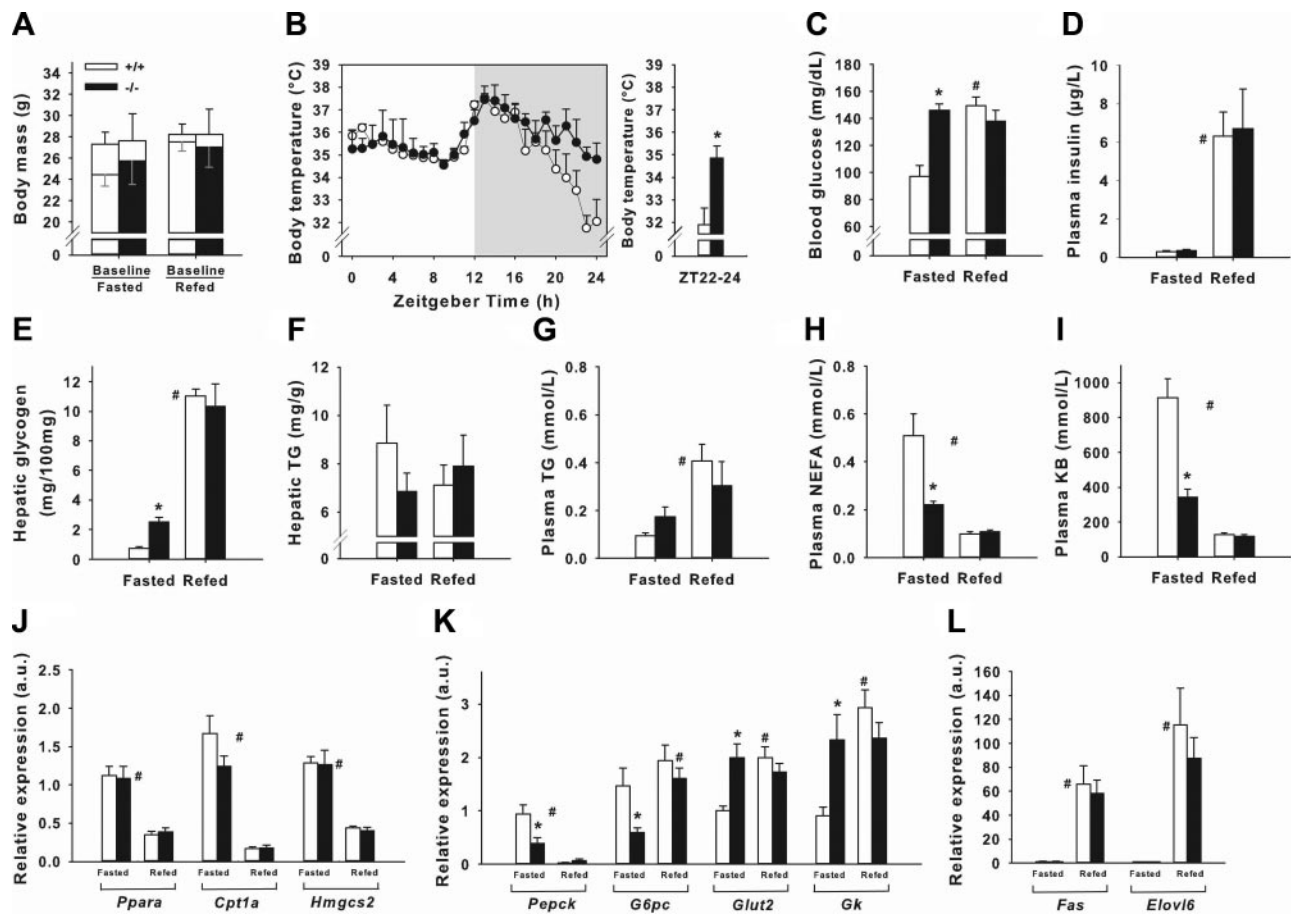
Figure 4. Shift from glucose to fatty acid utilization in unfed *Rev-erbα*$^{-/-}$ mice. *A*) Body mass changes determined before (left, upper values) and after a 24 h fast (left, lower values), and before (right, upper values) and after 24 h of food withdrawal + 24 h refeeding (right, lower values) in *Rev-erbα*$^{+/+}$ and *Rev-erbα*$^{-/-}$ mice. *B*) Body temperature during 24 h of food withdrawal and the adjacent ZT22-24 average. Open circles, *Rev-erbα*$^{+/+}$ mice; solid circles, *Rev-erbα*$^{-/-}$ mice. *C–I*) Blood glucose (*C*), plasma insulin (*D*), hepatic glycogen (*E*), hepatic triglyceride (TG; *F*), plasma TG (*G*), plasma NEFA (*H*), and plasma ketone body (KB; *I*) levels in unfed (fasted) and refed animals. *J–L*) mRNA expression levels of ketogenic genes (*J*), glucose metabolism genes (*K*), and lipogenic genes (*L*). Animals were sampled at ZT0. Values are expressed as means ± SE (*n*=7/group). See Supplemental Table S1 for gene names. $^{\#}P < 0.05$ for main effect of feeding condition (midpanel) or *vs.* corresponding unfed (fasted) group of same genotype (above bar); $*P < 0.05$ *vs.* +/+ genotype of same feeding condition.

NEFA and ketone body levels were significantly decreased in *Rev-erbα*$^{-/-}$ mice compared to control mice (Fig. 4*H*, *I*). This suggests that fatty acids are used as the main source of energy during 24 h of food withdrawal in *Rev-erbα*-deficient animals.

To substantiate this possibility, we analyzed the mRNA expression of *peroxisome proliferator-activated receptor* α (*Pparα*) and *Pparα*-target genes known to be involved in ketogenesis: *carnitine palmitoyltransferase 1a* (*Cpt1a*) and *3-hydroxy-3-methylglutaryl-CoA synthase 2* (*Hmgcs2*). Food withdrawal similarly enhanced the mRNA levels of *Pparα*, *Cpt1a*, and *Hmgcs2* in both genotypes (Fig. 4*J*), ruling out an abnormal ketogenesis in *Rev-erbα*$^{-/-}$ mice, which could have explained the reduction of their ketone body levels. In addition, the expression of *phosphoenolpyruvate carboxykinase 2* (*Pepck*) and *glucose-6-phosphatase* (*G6pc*), two key actors of gluconeogenesis, was reduced in unfed *Rev-erbα*$^{-/-}$ mice (Fig. 4*K*). Furthermore, the mRNA levels of *glucose transporter 2* (*Glut2*) and *glucokinase* (*Gk*), involved in glucose transport and both glycogen synthesis and

glycolysis, respectively, were higher after food withdrawal in *Rev-erbα*$^{-/-}$ mice than in wild-type mice (Fig. 4*K*). In contrast, loss of *Rev-erbα* did not block the refeeding-induced increase of lipogenic genes (Fig. 4*L* and Supplemental Fig. S4*C*). The mRNA levels of other regulators of glucose and lipid metabolism were similar between the genotypes (Supplemental Fig. S4*B*, *C*). To summarize, unfed *Rev-erbα*$^{-/-}$ mice maintain relative hyperglycemia, concomitant with available glycogen stores and reduced gluconeogenesis. In agreement with these findings, the lower RQ values in chow-fed *Rev-erbα*$^{-/-}$ mice during daytime demonstrate that *Rev-erbα* deletion *in vivo* leads to a greater mobilization and oxidation of fatty acids as well as a greater ketolysis during the resting period.

Rev-erbα$^{-/-}$ mice are more prone to HFD-induced obesity

The experiments reported above indicate that the absence of *Rev-erbα* leads to a shift from glucose to fatty

acid utilization for energy supply, at least during the resting period and 24 h of food withdrawal. During nighttime (*i.e.*, period of dietary carbohydrate intake), however, mild hyperglycemia, normal insulin sensitivity, and high RQ values in chow-fed *Rev-erbα*$^{-/-}$ mice indicate an active absorption of carbohydrates. We wondered whether *de novo* lipogenesis from dietary carbohydrates could be increased at night in *Rev-erbα*$^{-/-}$ mice. We first assessed day-night parameters related to lipid metabolism in 4-wk-old *Rev-erbα*$^{+/+}$ and $^{-/-}$ mice fed chow or HFD for up to 12 wk. *Rev-erbα*$^{-/-}$ mice fed HFD gained much more body mass than HFD-fed control animals (**Fig. 5A**). This cannot be attributed to biased (*i.e.*, different) values of baseline body mass, because they were similar between the genotypes at 4 wk of age. Moreover, all groups had a similar body size at the end of the experiments (data not shown). Mean calorie intake did not significantly differ between the genotypes, despite a trend for increased calorie consumption in the *Rev-erbα*$^{-/-}$ group ($P=0.08$; Supplemental Fig. S5*A*). *Rev-erbα*$^{-/-}$ mice had a significantly higher body mass index, especially in the HFD group (Supplemental Fig. S5*B*). In accordance with this observation, the amount of WAT (*i.e.*, perigonadal and retroperitoneal) was also significantly greater in *Rev-erbα*$^{-/-}$ mice compared to controls, regardless of the feeding conditions (Fig. 5*B, C*). As expected (33), HFD-fed control animals had significantly higher body mass and adiposity than chow-fed control animals, and in addition, they reached a similar adiposity as in chow-fed *Rev-erbα*$^{-/-}$ mice (Fig. 5*B, C*).

When fed HFD, both genotypes expressed an attenuated diurnal feeding rhythm (data not shown) and showed significant hyperleptinemia (Fig. 5*D*), increased hepatic triglycerides (Fig. 5*F*), decreased plasma triglycerides (Fig. 5*G*), increased plasma LDL and plasma NEFAs (Fig. 5*H, I*), hypercholesterolemia (Supplemental Fig. S5*D*) and hyperinsulinemia (Supplemental Fig. S5*G*), compared to their chow-fed controls. Interestingly, irrespective of the feeding conditions, *Rev-erbα*$^{-/-}$ mice had significantly increased plasma leptin, glucose, NEFA, LDL, ketone body, cholesterol, insulin, and adiponectin levels compared to *Rev-erbα*$^{+/+}$ mice (Fig. 5*D, E, H–J* and Supplemental Fig. S5*D, G, H*). Incidentally, HFD-induced hyperglycemia was only detected with blood sampling by tail incision (Supplemental Fig. S5*K, L*). The high levels of adiponectin and leptin in chow- and HFD-fed *Rev-erbα*$^{-/-}$ mice could have prevented the development of insulin resistance (34). Corticosterone levels, important for carbohydrate metabolism, were not significantly enhanced in chow-fed *Rev-erb*$^{-/-}$ mice (Supplemental Fig. S5*I*). Hepatic triglycerides in chow-fed *Rev-erbα*$^{-/-}$ mice were found to be increased at ZT10 (20) and reduced at ZT12 (25). However, we noticed a trend toward elevated hepatic triglycerides at ZT12 in *Rev-erbα*$^{-/-}$ mice, regardless of the feeding conditions ($P=0.06$; Fig. 5*F*). Of interest, plasma glycerol in *Rev-erbα*$^{-/-}$ mice was enhanced at ZT12 in chow-fed conditions and at both time points in HFD-fed conditions (Supplemental Fig. S5*F*), which may indicate enhanced hydrolysis of triglycerides. Taken together, our data indicate that *Rev-erbα* deletion leads to a fat phenotype in chow-fed conditions, which is severely amplified in HFD-fed conditions.
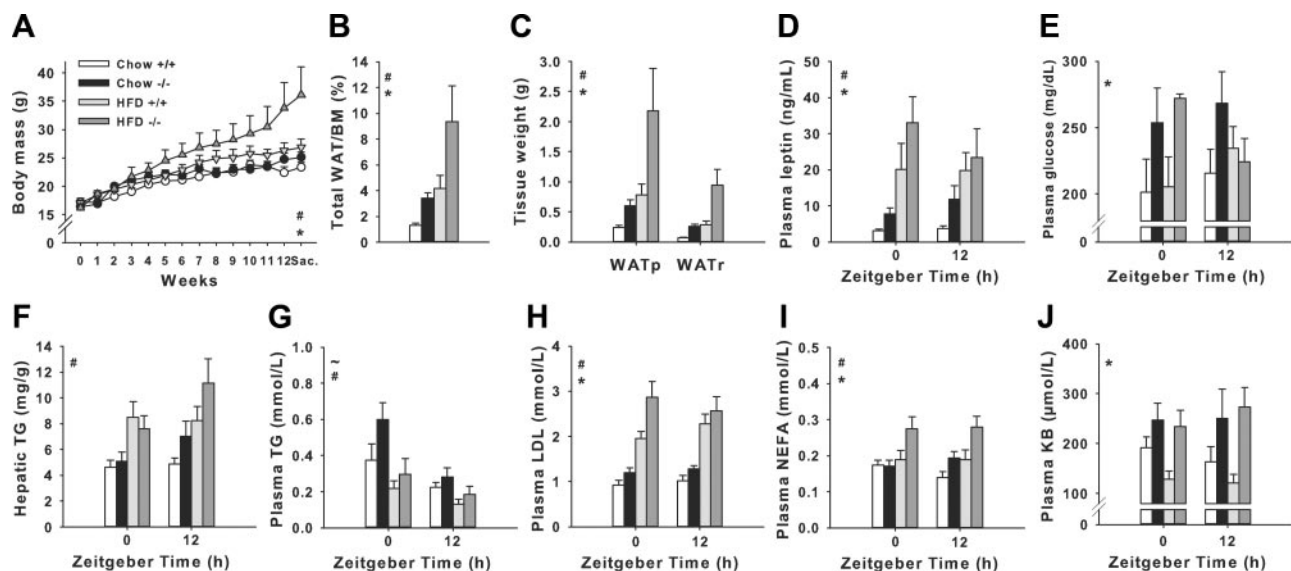

Figure 5. *Rev-erbα*$^{-/-}$ mice exhibit a fat phenotype amplified on prolonged high-fat feeding. *A*) Body mass change over time in chow-fed and HFD-fed +/+ and −/− animals (*n*=12/group). Sac., sacrifice. Note that statistical analysis was performed on the last week of feeding. Open circles, chow-fed *Rev-erbα*$^{+/+}$ mice; solid circles, chow-fed *Rev-erbα*$^{-/-}$ mice; light shaded triangles, HFD-fed *Rev-erbα*$^{+/+}$ mice; dark shaded triangles, HFD-fed *Rev-erbα*$^{-/-}$ mice. *B*) Total adiposity, expressed as a percentage of body mass (*n*=12/group). *C*) Amount of perigonadal and retroperitoneal WAT (WATp and WATr, respectively; *n*=12/group). *D, E*) Plasma leptin (*D*) and glucose (*E*) levels (*n*=6/group). *F, G*) Hepatic triglyceride (TG; *F*) and plasma TG (*G*) levels (*n*=6/group). *H–J*) Plasma LDL (*H*), NEFA (*I*), and ketone body (KB; *J*) levels (*n*=6/group). Values are expressed as means ± sᴇ. $^{\sim}P < 0.05$ for main effect of time; $*P < 0.05$ for main effect of genotype; $^{\#}P < 0.05$ for main effect of feeding condition.

Expression of metabolic genes is disrupted in chow- and HFD-fed Rev-erbα^{−/−} mice

To gain further insight into the role of REV-ERBα as transcriptional repressor for the daily control of energy balance, we examined the day-night levels of glucose and lipid-related genes in the liver, WAT, and skeletal muscle of chow- and HFD-fed Rev-erbα+/+ and −/− mice. Of note, day-night expression patterns of most metabolic genes studied in Rev-erbα+/+ mice were in accordance with expression profiling from transcriptome data (10,35). We first determined whether the defective energy homeostasis in Rev-erbα−/− mice was the consequence of altered hepatic gene expression. Notably, hepatic *glycogen synthase 2* (*Gys2*) and *Glut2* expression was significantly diminished at ZT12 in Rev-erbα−/− mice in both feeding conditions (**Fig. 6A**), while no significant differences were found for *Gk*,

Pepck, and *G6pc* (Supplemental Fig. S6A), in keeping with a previous report (20). Hepatic expression of lipogenic genes [*e.g.*, *sterol regulatory element binding transcription factor 1* (*Srebp1c*) and *fatty acid synthase* (*Fas*)] showed decreased levels at ZT12 in chow-fed Rev-erbα−/− mice (Fig. 6A). However, while HFD did not markedly change the expression of *Srebp1c*, the hepatic mRNA levels of *Fas*, *acetyl-coenzyme A carboxylase* (*Acc*), and *ELOVL fatty acid elongase 6* (*Elovl6*) in the Rev-erbα−/− group were ~2-fold higher than in control animals at both time points (Fig. 6A). Similarly, we found that the fatty acid transporter *cluster of differentiation 36* (*Cd36*) was significantly induced by HFD exclusively in Rev-erbα−/− animals (Fig. 6A). Of special interest, *Lpl* mRNA, which encodes the rate-limiting enzyme in triglyceride hydrolysis (36), was significantly increased at ZT12 in the liver of Rev-erbα−/− mice
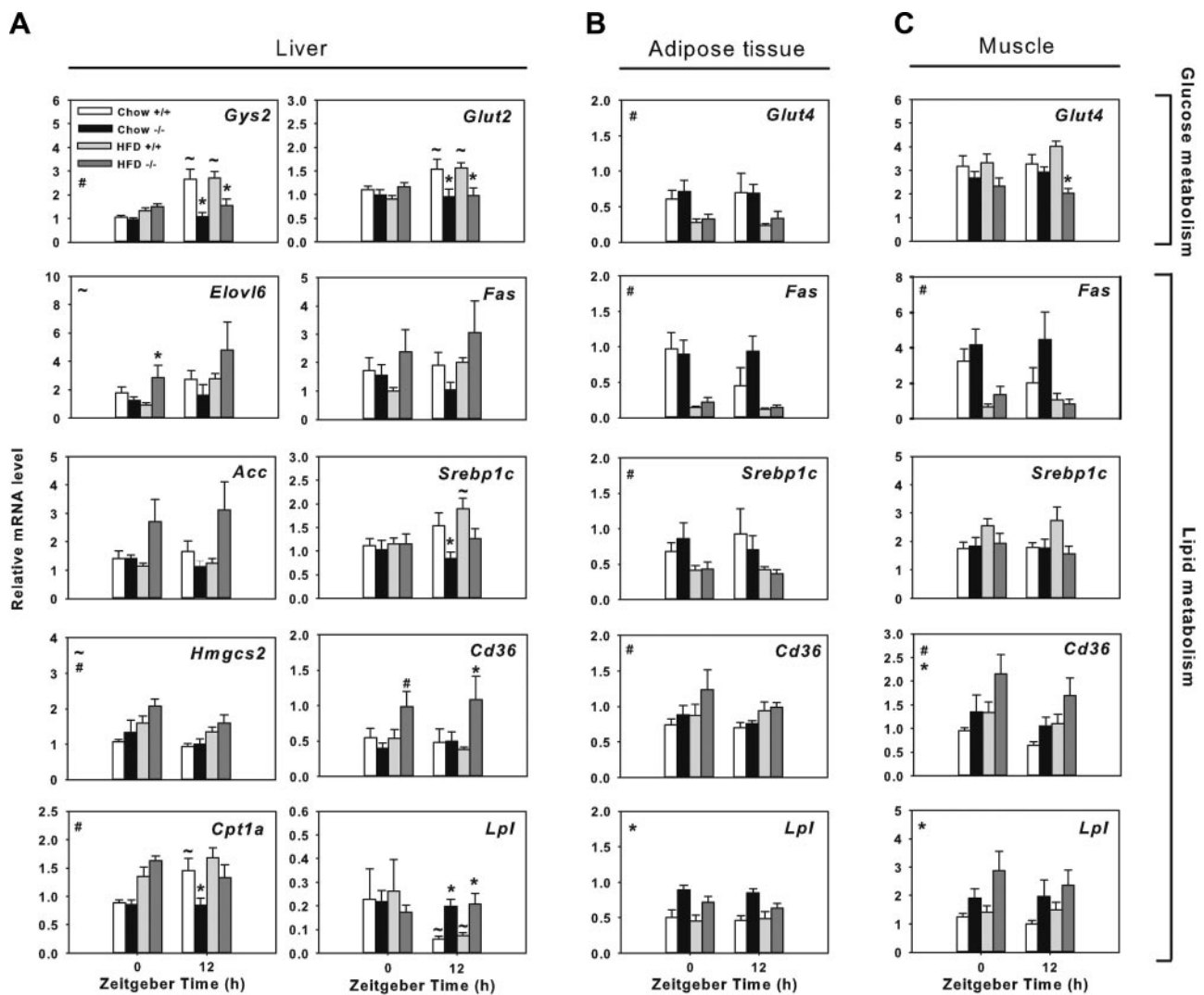

Figure 6. Lipid metabolism gene expression is modified in the absence of Rev-erbα. mRNA expression of glucose and lipid metabolism genes in liver (*A*), retroperitoneal WAT (*B*), and rectus femoris skeletal muscle (*C*). Data are means ± SE (*n*=6/group). See Supplemental Table S1 for gene names. ~*P* < 0.05 for main effect of time (top left corner) or *vs.* corresponding ZT0 group of same genotype (above bar); *P* < 0.05 for main effect of genotype (top left corner) or *vs.* corresponding +/+ genotype at same ZT and feeding condition (above bar); #*P* < 0.05 for main effect of feeding condition (top left corner) or *vs.* corresponding chow-fed group at same ZT (above bar).

compared to controls (Fig. 6A). Taken together, the elevated expression of these metabolic actors may contribute to obesity.

To further specify the obesity phenotype of *Rev-erbα*$^{-/-}$ mice, we analyzed the mRNA levels of metabolic actors in WAT and skeletal muscle. *Glut4*, *Fas*, *Acc*, and *Srebp1c* were significantly down-regulated by HFD in both genotypes (Fig. 6B and Supplemental Fig. S6B). Incidentally, this HFD-dependent regulation of the lipogenic genes *Acc* and *Fas* has also been observed in obese humans and rodents (37). While there was no difference in *Cd36* expression between the two genotypes, the deletion of *Rev-erbα* also increased *Lpl* mRNA expression in WAT (Fig. 6B). This suggests that in *Rev-erbα*$^{-/-}$ mice, WAT *Lpl* enhanced uptake of NEFA for fat storage, thus contributing to fat overload. In skeletal muscle, an overall tendency to down-regulate *Glut4* was seen in *Rev-erbα*$^{-/-}$ mice, which only reached statistical significance in HFD-fed *Rev-erbα*$^{-/-}$ animals at ZT12 (Fig. 6C), when massive body fat overload started to impede physical activity (data not shown). Expression of *Fas* and *Acc* in the muscle was also down-regulated in response to HFD in both genotypes, whereas the expression of *Cd36* was increased by HFD in both genotypes (Fig. 6C, Supplemental S6C). Of note, *Cd36* and *Lpl* expression was significantly increased in *Rev-erbα*$^{-/-}$ mice, irrespective of the feeding conditions (Fig. 6C). This further supports our hypothesis of an enhanced utilization of fatty acids as energy substrate for the muscle.

Altogether, these results clearly indicate that *Rev-erbα*$^{-/-}$ mice display a defective molecular control of energy homeostasis which contributes to HFD-induced obesity. Both liver and skeletal muscle appear to play a role in the production and preferential use of fatty acids at the expense of peripheral utilization of glucose, thus leading to a chronic mild hyperglycemia.

CLOCK drives transcriptional activation of *Lpl*

The overexpression of *Lpl* mRNA that we found in 3 peripheral tissues of *Rev-erbα*$^{-/-}$ mice led us to test whether this gene could be clock controlled. Since several putative RORE motifs were found in the proximal promoter region of *Lpl* (see Supplemental Data), we first decided to check whether the latter would be responsive to REV-ERBα and RORα. Neither RORα nor REV-ERBα had any effect toward this reporter construct (**Fig. 7A**). In contrast, RORα consistently activated *Bmal1-luc*, an effect that could be partially overcome by the addition of REV-ERBα (Fig. 7B).

However, the transcriptions of *Rev-erbα* and *Clock/ Bmal1* are interlocked: The heterodimer CLOCK/ BMAL1 drives *Rev-erbα* transcription (38), and REV-ERBα inhibits both *Bmal1* and *Clock* transcriptions, as previously mentioned. This explains why the mRNA levels of both *Bmal1* and *Clock* are higher in the *Rev-erbα*$^{-/-}$ mice than in their wild-type littermates (Supplemental Fig. S7). Therefore, it seems plausible that at least a subset of CLOCK/BMAL1 targets will
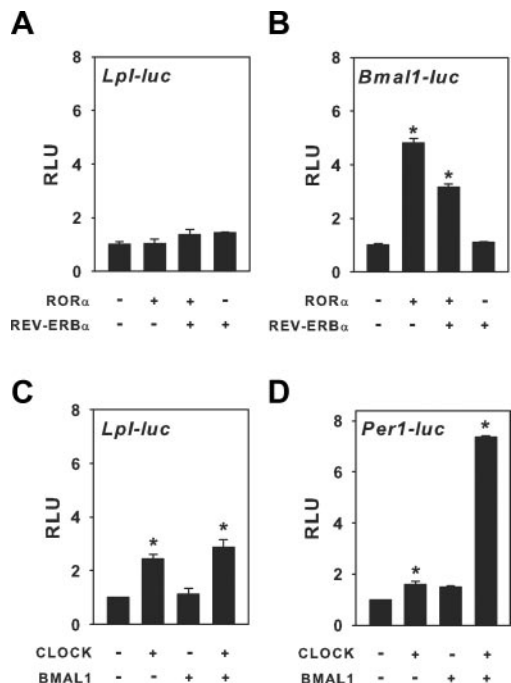
Figure 7. Transactivation by CLOCK of the *Lpl* promoter. *A, B*) Effects of RORα and REV-ERBα on the transcription of *Lpl-luc* (*A*) and *Bmal1-luc* (*B*) promoter reporter constructs. *C, D*) Effects of CLOCK and BMAL1 on the transcription of *Lpl-luc* (*C*) and *Per1-luc* (*D*) promoter reporter constructs. Luciferase assay was performed on COS-7 cells as indicated in Materials and Methods. Data are means ± SE of a representative experiment performed in triplicate wells. RLU, relative luminescence units. *$P < 0.05$ *vs.* control (empty vector).

display enhanced expression levels in these *Rev-erbα*$^{-/-}$ mice. We thus tested the potential implication of a putative E-box, which is located in the most proximal promoter region of m*Lpl*. This reporter construct significantly responded to CLOCK/BMAL1, although the amplitude of the response was not different from that elicited by CLOCK alone (Fig. 7C). These results demonstrate that the circadian clockwork is somehow involved in the transcriptional activation of the *Lpl* gene.

DISCUSSION

Energy metabolism can be affected by circadian disturbance, as evidenced by epidemiologic studies in shift workers and genetic disruption of clock components in mice (1, 11). REV-ERBα is a transcription factor involved both in the molecular clockwork and in several metabolic pathways. Therefore, dissecting REV-ERBα contribution to the daily balance between glucose and lipid metabolism is an important step toward understanding the functional crosstalk between the circadian and metabolic systems. Here we show that the absence of REV-ERBα *in vivo* leads to a preferential use of fatty acids as energy substrate during daytime, in association with non-insulin-dependent hyperglycemia.

During the daily resting period, liver and muscle derive most of their energy from fatty acids released

from WAT. Chow-fed *Rev-erbα*$^{-/-}$ mice rely more on lipid fuels during the inactive period than do control mice, as evidenced by low (*i.e.*, close to 0.7) RQ values. Accordingly, hepatic glycogen is less mobilized at the end of the resting period, while the hyperglycemia persists. A defect of glucose entry due to tissue-specific impaired insulin signaling would have explained the increased fatty acid utilization in *Rev-erbα*$^{-/-}$ mice. Deficiency in *Glut4* expression has been associated with insulin resistance (39). However, chow-fed *Rev-erbα*$^{-/-}$ mice have normal whole-body insulin sensitivity without obvious changes in *Glut4* mRNA levels in peripheral tissues.

Another explanation for the increased fatty acid utilization stems from the implication of REV-ERBα in the regulation of myosin heavy chain (MyHc) isoform expression in the skeletal muscle, based in particular on a significant fast-to-slow MyHC isoform transformation in skeletal muscle of *Rev-erbα*$^{-/-}$ mice (40). Thus, the preponderance of this slow myosin may have increased aerobic lipid metabolism, sparing glucose use in the muscles of *Rev-erbα*-deficient mice. In agreement with this hypothesis, the membrane protein *Cd36* involved in the binding and transport of fatty acids (36) is up-regulated in *Rev-erbα*$^{-/-}$ mice in the rectus femoris muscle, which has both oxidative and glycolytic capabilities (41). Muscle-specific overexpression of *Cd36* in mice promotes clearance of circulating fatty acids and increases plasma glucose and insulin (42). Furthermore, *Lpl* mRNA in the muscle of *Rev-erbα*-deficient animals is up-regulated both in the morning and the evening. Of note, LPL activity is higher in muscles composed predominantly of high-oxidative slow-twitch fibers (43) and is inversely phased to daily variation of RQ (44). Moreover, *Rev-erbα*$^{-/-}$ mice are resistant to cold-induced hypothermia (Supplemental Fig. S8), as are transgenic mice that overexpress *Lpl* in skeletal muscles (45). This improved cold tolerance could be linked to changes in muscle physiology (*i.e.*, enhanced oxidative capacity) due to LPL overexpression (45). Taken together, these findings show that increased *Cd36* and *Lpl* expression reflects increased muscular uptake of fatty acids in *Rev-erbα*$^{-/-}$ mice and can contribute not only to hyperglycemia but also to the absence of food withdrawal-induced drops in blood glucose and body temperature.

The physiological responses to acute food withdrawal include depletion of glycogen stores, hepatic gluconeogenesis, and mobilization of triglyceride in adipose tissues, which together provide energy supply. After 24 h of food withdrawal, glycogen depletion in *Rev-erbα*$^{-/-}$ mice remains incomplete and the hepatic expression of gluconeogenic genes much less increased in their liver. Strikingly, blood glucose levels in unfed *Rev-erbα*$^{-/-}$ mice are not decreased as in control animals, but instead show similar values to those of fed *Rev-erbα*$^{-/-}$ mice. In sharp contrast, plasma NEFA and ketone bodies levels in unfed *Rev-erbα*$^{-/-}$ mice are lower than in unfed control mice, reflecting acute utilization of fatty acids. This conclusion is substantiated by the facts that plasma NEFA and ketone body levels are either similar or greater in chow-fed *Rev-erbα*$^{-/-}$ mice compared to their controls, and that ketogenesis at the molecular level is induced by food withdrawal. Thus, it is unlikely that reduced NEFA and ketone bodies levels are due to decreased lipolysis and ketogenesis. Hence, the relative hyperglycemia and normothermia in starved *Rev-erbα*$^{-/-}$ mice result from a combination of lower activation of gluconeogenesis, diminished glucose utilization, and increased production and utilization of lipid fuels.

During the daily activity period, feeding allows the restoration of energy stores depleted over the previous daytime resting period. Nocturnal RQ values in *Rev-erbα*$^{-/-}$ mice are higher than in control mice, suggesting a greater utilization of glucose. This feature, however, cannot be explained by increased *Glut4* mRNA levels, fast glycolytic fibers (40), or physical activity. Alternatively, higher nocturnal RQ values in *Rev-erbα*$^{-/-}$ mice can result from increased *de novo* lipogenesis, leading to enhanced production of lipids. Indeed, when fatty acids are synthesized from glucose, for instance during the absorption of dietary carbohydrates, the average RQ remains close to or below 1 (46). *Rev-erbα*$^{-/-}$ mice exhibit increased adiposity even when fed chow. Of note, body fat can derive from dietary fat and *de novo* lipogenesis, mainly from carbohydrates (46). *Fas* mRNA expression shows a 2-fold increase at ZT12 in the muscle and WAT of *Rev-erbα*$^{-/-}$ mice, indicating elevated fat synthesis in these tissues. However, no increased expression of lipogenic genes has been detected in the liver of chow-fed *Rev-erbα*$^{-/-}$ mice. This is explained by our sampling times, because expression of *Srebp1c*, *Fas*, and *Elovl6* is phase shifted in the liver of *Rev-erbα*-deficient mice (20), suggesting a delay in the occurrence of fat synthesis. This was confirmed by Feng *et al.* (25), who demonstrated that REV-ERBα controls the expression of lipid metabolism genes by recruiting the repressive chromatin modifier histone deacetylase 3, ensuring a temporal control of lipogenesis. In line with this study, we also show a trend toward elevated hepatic triglycerides, an important source of lipids for very low density lipoprotein (VLDL) assembly at the end of the day. Hepatic *de novo* lipogenesis contributes to VLDL production, the latter being increased in *Rev-erbα*-deficient mice (47). In addition, our calorimetry data indicating a possible nocturnal elevation of fat synthesis from dietary glucose in chow-fed *Rev-erbα*$^{-/-}$ mice are in accordance with an increased *de novo* lipogenesis found in these mice following the administration of deuterated water (25). The improved ability to convert dietary glucose to fat in the absence of *Rev-erbα* may explained the diminished differences in blood glucose levels between both genotypes fed high-carbohydrate diet or HFD.

In addition, our study demonstrates that the altered circadian control of lipid homeostasis due to the absence of REV-ERBα *in vivo* facilitates HFD-induced obesity. The metabolic phenotype in *Rev-erbα*$^{-/-}$ mice is robust, as increased adiposity occurs even on chow

diet without significant hyperphagia. Interestingly, an opposite phenotype (*i.e.*, resistance to HFD) has been described in *Rorα*-deficient mice (48). While *Rev-erbα*^{+/+} and *Rev-erbα*^{−/−} mice challenged with HFD become overweight and develop hyperleptinemia, hyperlipidemia, hypercholesterolemia, hyperinsulinemia, and fatty liver, these metabolic responses are all significantly greater in *Rev-erbα*^{−/−} mice. Besides, high-fat-fed *Rev-erbα*^{−/−} mice display increased ketonemia, which is likely a response to an overload of the citric acid cycle, blood glucose being converted to acetyl-CoA in parallel to the production of acetyl-CoA from fat breakdown. This indicates that the enhancement of the fat oxidation capacity of the skeletal muscle of *Rev-erbα*^{−/−} mice is not sufficient to cope with the adverse effects of prolonged HFD feeding. In addition, hepatic expression of *Acc*, *Fas*, and *Elovl6* increases only in *Rev-erbα*^{−/−} mice at both time points on HFD, in keeping with increased *de novo* lipogenesis.

The overexpression of *Lpl* observed in *Rev-erbα*^{−/−} mice is not restricted to the skeletal muscle. Indeed, expression of *Lpl*, which is barely detectable in the adult liver (49), is significantly up-regulated at ZT12 in the liver of *Rev-erbα*^{−/−} mice. This is in line with the 24-h up-regulation of the *Lpl* transcript found in these mice by Le Martelot *et al.* (20). Of note, hepatic *endothelial lipase* mRNA levels are decreased in the liver (20) while *hepatic lipase* mRNA expression is similar in *Rev-erbα*^{−/−} mice (Supplemental Fig. S6). Interestingly, the metabolic phenotype of chow-fed *Rev-erbα*^{−/−} animals is quite similar to that of liver-only *Lpl*-expressing mice, which show increased liver triglyceride content and ketone body levels (50, 51). However, *Rev-erbα*^{−/−} mice do not exhibit insulin resistance like mice overexpressing *Lpl* in liver or skeletal muscle (51). Of importance, conflicting results have been reported regarding insulin resistance induced by *Lpl* overexpression (52). In addition, our results show that the overexpression of
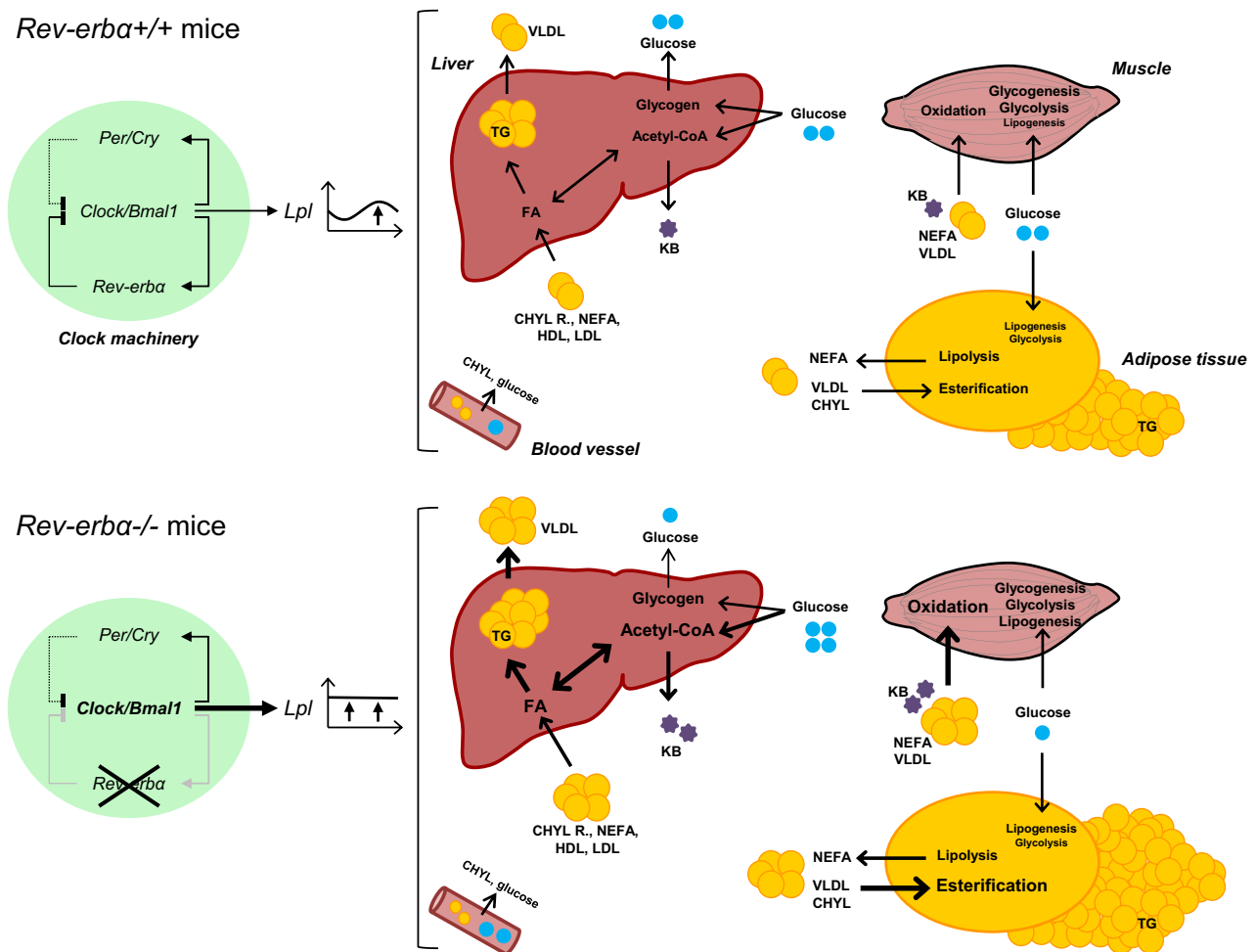

Figure 8. Hypothetical model illustrating the consequence of altered *Lpl* expression in *Rev-erbα*^{−/−} mice. In addition to altered daily hepatic expression of lipogenic genes (20, 25), *Rev-erbα* deletion impaired circadian control of *Lpl*, leading to its overexpression in peripheral tissues. As a result, skeletal muscle may adapt by preferentially utilizing fatty acids (FA), thus sparing glucose. The surplus of glucose is therefore converted to acetyl-CoA through *de novo* lipogenesis in parallel to the generation of acetyl-CoA from fat breakdown. Acetyl-CoA production exceeding the cellular energy needs, ketone bodies (KB) are synthesized to make use of the energy available (*e.g.*, by muscle). At the same time, fat storage is increased as triglycerides (TG) in both liver and adipose tissue. This leads to a frail energy balance in which greater uptake of fatty acids by the muscle may relatively protect from severe hepatic steatosis and body fat overload. CHYL, chylomicrons; CHYL R, chylomicron remnants.

Lpl also occurs in WAT of *Rev-erbα*$^{-/-}$ mice. Specific overexpression of *Lpl* in adipose tissue does not lead to increased adiposity, an effect that could be due to down-regulation of LPL in other tissues or increase in energy expenditure (53). Interestingly, *Rev-erbα*$^{-/-}$ mice do not show increased body temperature, basal metabolism, or thermogenic response to noradrenaline (data not shown). Moreover, a direct correlation between adipocyte-derived LPL expression and lipid storage has been proposed (54). Therefore, it is likely that increased *Lpl* transcription in WAT of *Rev-erbα*$^{-/-}$ mice reflects increased activity of LPL, leading to enhanced hydrolysis of circulating triglycerides and facilitated NEFA uptake for storage.

The potential implication of REV-ERBα in the transcriptional control of *Lpl* was assessed by luciferase assay using the proximal promoter region of this gene. In contrast to a *Bmal1-luc* reporter, *mLpl-luc* was unresponsive to either REV-ERBα or RORα. Of interest, an E-box has been found in the mouse *Lpl* promoter (55). Instead of a direct repression by REV-ERBα, activation by CLOCK/BMAL1 could drive the temporal expression of the *Lpl* gene. Indeed, REV-ERBα expression is crucial on a daily basis for the transcriptional control of *Clock* and *Bmal1*. In the absence of *Rev-erbα*, *Clock* and *Bmal1* mRNA are overexpressed in peripheral tissues, which can affect the expression of CLOCK/BMAL1 target genes. Our results show that *Lpl* expression can be elicited by CLOCK alone. Whether this effect depends on the acetyltransferase activity of CLOCK (56,57) remains to be established. Such a positive regulation of *Lpl* transcription by CLOCK/BMAL1 has been previously mentioned (J. M. Gimble and Z. E. Floyd, Pennington Biomedical Research Center, Baton Rouge, LA, USA; unpublished results mentioned in ref. 58). Thus, the overexpression of *Lpl* appears to be the result of a defective clockwork, keeping in mind that the regulation of *Lpl* transcription can also be achieved by other pathways (59, 60).

This study provides strong insight into the role of REV-ERBα in the regulation of *in vivo* energy balance. Our findings do not fully exclude the possibility that impaired development of skeletal muscles (40) and adipocytes (19) in *Rev-erbα*-deficient mice may participate in the observed metabolic phenotype. Alternatively, altered clock functioning in the absence of REV-ERBα could account for impaired temporal coordination of developmental processes related to muscle and adipose physiology (58, 61). We propose that altered circadian control of metabolic pathways across peripheral tissues is likely the main cause of the metabolic phenotype of the *Rev-erbα*$^{-/-}$ mice. Our data are in agreement with the involvement of REV-ERBα in the timing of hepatic lipid metabolism genes (20, 25). Furthermore, we show that altered clock machinery leads to up-regulated transcription of *Lpl*. In line with a clock-regulated timing of *Lpl* mRNA expression, we could not detect day-night variation of *Lpl* in the liver of *Rev-erbα*$^{-/-}$ mice. Circadian variations of *Lpl* mRNA and LPL activity have been observed in various tissues including the liver, with hepatic mRNA acrophase in the early morning (4, 10, 20, 44, 59). Therefore, in the context of glucose and fat regulation, circadian control of *Lpl* appears to be essential for a balanced energy metabolism, as suggested by Gimble and Floyd (58). If *Lpl* is expressed continuously around the clock, fat overload can ensue, while at the same time muscles adapt toward a more oxidative metabolism (**Fig. 8**).

In summary, the present study uncovers a molecular pathway that ties clock-driven *Lpl* expression to energy homeostasis and highlights circadian disruption as a potential cause for the etiology of the metabolic syndrome. [FJ]

REFERENCES

1. Froy, O. (2010) Metabolism and circadian rhythms–implications for obesity. *Endocr. Rev.* **31,** 1–24
2. Kalsbeek, A., Yi, C. X., La Fleur, S. E., and Fliers, E. (2010) The hypothalamic clock and its control of glucose homeostasis. *Trends Endocrinol. Metab.* **21,** 402–410
3. Asher, G., and Schibler, U. (2011) Crosstalk between components of circadian and metabolic cycles in mammals. *Cell Metab.* **13,** 125–137
4. Zvonic, S., Ptitsyn, A. A., Conrad, S. A., Scott, L. K., Floyd, Z. E., Kilroy, G., Wu, X., Goh, B. C., Mynatt, R. L., and Gimble, J. M. (2006) Characterization of peripheral circadian clocks in adipose tissues. *Diabetes* **55,** 962–970
5. Shibata, S., Tahara, Y., and Hirao, A. (2010) The adjustment and manipulation of biological rhythms by light, nutrition, and abused drugs. *Adv. Drug Deliv. Rev.* **62,** 918–927
6. Ko, C. H., and Takahashi, J. S. (2006) Molecular components of the mammalian circadian clock. *Hum. Mol. Genet.* **15**(Spec. 2), R271–R277
7. Guillaumond, F., Dardente, H., Giguere, V., and Cermakian, N. (2005) Differential control of Bmal1 circadian transcription by REV-ERB and ROR nuclear receptors. *J. Biol. Rhythms.* **20,** 391–403
8. Preitner, N., Damiola, F., Lopez-Molina, L., Zakany, J., Duboule, D., Albrecht, U., and Schibler, U. (2002) The orphan nuclear receptor REV-ERBalpha controls circadian transcription within the positive limb of the mammalian circadian oscillator. *Cell* **110,** 251–260
9. Crumbley, C., and Burris, T. P. (2011) Direct regulation of CLOCK expression by REV-ERB. *PLoS One* **6,** e17290
10. Panda, S., Antoch, M. P., Miller, B. H., Su, A. I., Schook, A. B., Straume, M., Schultz, P. G., Kay, S. A., Takahashi, J. S., and Hogenesch, J. B. (2002) Coordinated transcription of key pathways in the mouse by the circadian clock. *Cell* **109,** 307–320

11. Delezie, J., and Challet, E. (2011) Interactions between metabolism and circadian clocks: reciprocal disturbances. *Ann. N. Y. Acad. Sci.* **1243,** 30–46

12. Turek, F. W., Joshu, C., Kohsaka, A., Lin, E., Ivanova, G., McDearmon, E., Laposky, A., Losee-Olson, S., Easton, A., Jensen, D. R., Eckel, R. H., Takahashi, J. S., and Bass, J. (2005) Obesity and metabolic syndrome in circadian Clock mutant mice. *Science* **308,** 1043–1045

13. Marcheva, B., Ramsey, K. M., Buhr, E. D., Kobayashi, Y., Su, H., Ko, C. H., Ivanova, G., Omura, C., Mo, S., Vitaterna, M. H., Lopez, J. P., Philipson, L. H., Bradfield, C. A., Crosby, S. D., JeBailey, L., Wang, X., Takahashi, J. S., and Bass, J. (2010) Disruption of the clock components CLOCK and BMAL1 leads to hypoinsulinaemia and diabetes. *Nature* **466,** 627–631

14. Mendoza, J., Pevet, P., and Challet, E. (2008) High-fat feeding alters the clock synchronization to light. *J. Physiol.* **586,** 5901–5910

15. Kohsaka, A., Laposky, A. D., Ramsey, K. M., Estrada, C., Joshu, C., Kobayashi, Y., Turek, F. W., and Bass, J. (2007) High-fat diet disrupts behavioral and molecular circadian rhythms in mice. *Cell Metab.* **6,** 414–421

16. Dallmann, R., and Weaver, D. R. (2010) Altered body mass regulation in male mPeriod mutant mice on high-fat diet. *Chronobiol. Int.* **27,** 1317–1328

17. Lazar, M. A., Hodin, R. A., Darling, D. S., and Chin, W. W. (1989) A novel member of the thyroid/steroid hormone receptor family is encoded by the opposite strand of the rat c-erbA alpha transcriptional unit. *Mol. Cell. Biol.* **9,** 1128–1136

18. Vieira, E., Marroqui, L., Batista, T. M., Caballero-Garrido, E., Carneiro, E. M., Boschero, A. C., Nadal, A., and Quesada, I. (2012) The clock gene Rev-erbalpha regulates pancreatic beta-cell function: modulation by leptin and high-fat diet. *Endocrinology* **153,** 592–601

19. Wang, J., and Lazar, M. A. (2008) Bifunctional role of Rev-erbalpha in adipocyte differentiation. *Mol. Cell. Biol.* **28,** 2213–2220

20. Le Martelot, G., Claudel, T., Gatfield, D., Schaad, O., Kornmann, B., Sasso, G. L., Moschetta, A., and Schibler, U. (2009) REV-ERBalpha participates in circadian SREBP signaling and bile acid homeostasis. *PLoS Biol* **7,** e1000181

21. Duez, H., van der Veen, J. N., Duhem, C., Pourcet, B., Touvier, T., Fontaine, C., Derudas, B., Bauge, E., Havinga, R., Bloks, V. W., Wolters, H., van der Sluijs, F. H., Vennstrom, B., Kuipers, F., and Staels, B. (2008) Regulation of bile acid synthesis by the nuclear receptor Rev-erbalpha. *Gastroenterology* **135,** 689–698

22. Yin, L., Wu, N., Curtin, J. C., Qatanani, M., Szwergold, N. R., Reid, R. A., Waitt, G. M., Parks, D. J., Pearce, K. H., Wisely, G. B., and Lazar, M. A. (2007) Rev-erbalpha, a heme sensor that coordinates metabolic and circadian pathways. *Science* **318,** 1786–1789

23. Wu, N., Yin, L., Hanniman, E. A., Joshi, S., and Lazar, M. A. (2009) Negative feedback maintenance of heme homeostasis by its receptor, Rev-erbalpha. *Genes Dev.* **23,** 2201–2209

24. Raghuram, S., Stayrook, K. R., Huang, P., Rogers, P. M., Nosie, A. K., McClure, D. B., Burris, L. L., Khorasanizadeh, S., Burris, T. P., and Rastinejad, F. (2007) Identification of heme as the ligand for the orphan nuclear receptors REV-ERBalpha and REV-erbbeta. *Nat. Struct. Mol. Biol.* **14,** 1207–1213

25. Feng, D., Liu, T., Sun, Z., Bugge, A., Mullican, S. E., Alenghat, T., Liu, X. S., and Lazar, M. A. (2011) A circadian rhythm orchestrated by histone deacetylase 3 controls hepatic lipid metabolism. *Science* **331,** 1315–1319

26. Fergani, A., Eschbach, J., Oudart, H., Larmet, Y., Schwalenstocker, B., Ludolph, A. C., Loeffler, J. P., and Dupuis, L. (2011) A mutation in the dynein heavy chain gene compensates for energy deficit of mutant SOD1 mice and increases potentially neuroprotective IGF-1. *Mol. Neurodegener.* **6,** 26

27. Heikkinen, S., Argmann, C. A., Champy, M. F., and Auwerx, J. (2007) Evaluation of glucose homeostasis. *Curr. Protoc. Mol. Biol.* Chap. 29, Unit 29B 23

28. Murat, J. C., and Serfaty, A. (1974) Simple enzymatic determination of polysaccharide (glycogen) content of animal tissues. *Clin. Chem.* **20,** 1576–1577

29. Miao, B., Zondlo, S., Gibbs, S., Cromley, D., Hosagrahara, V. P., Kirchgessner, T. G., Billheimer, J., and Mukherjee, R. (2004) Raising HDL cholesterol without inducing hepatic steatosis and hypertriglyceridemia by a selective LXR modulator. *J. Lipid Res.* **45,** 1410–1417

30. Dardente, H., Fustin, J. M., and Hazlerigg, D. G. (2009) Transcriptional feedback loops in the ovine circadian clock. *Comp. Biochem. Physiol. A Mol. Integr. Physiol.* **153,** 391–398

31. Travnickova-Bendova, Z., Cermakian, N., Reppert, S. M., and Sassone-Corsi, P. (2002) Bimodal regulation of mPeriod promoters by CREB-dependent signaling and CLOCK/BMAL1 activity. *Proc. Natl. Acad. Sci. U. S. A.* **99,** 7728–7733

32. Schmutz, I., Ripperger, J. A., Baeriswyl-Aebischer, S., and Albrecht, U. (2010) The mammalian clock component PERIOD2 coordinates circadian output by interaction with nuclear receptors. *Genes Dev.* **24,** 345–357

33. Gallou-Kabani, C., Vige, A., Gross, M. S., Rabes, J. P., Boileau, C., Larue-Achagiotis, C., Tome, D., Jais, J. P., and Junien, C. (2007) C57BL/6J and A/J mice fed a high-fat diet delineate components of metabolic syndrome. *Obesity (Silver Spring)* **15,** 1996–2005

34. Yamauchi, T., Kamon, J., Waki, H., Terauchi, Y., Kubota, N., Hara, K., Mori, Y., Ide, T., Murakami, K., Tsuboyama-Kasaoka, N., Ezaki, O., Akanuma, Y., Gavrilova, O., Vinson, C., Reitman, M. L., Kagechika, H., Shudo, K., Yoda, M., Nakano, Y., Tobe, K., Nagai, R., Kimura, S., Tomita, M., Froguel, P., and Kadowaki, T. (2001) The fat-derived hormone adiponectin reverses insulin resistance associated with both lipoatrophy and obesity. *Nat. Med.* **7,** 941–946

35. Hughes, M. E., DiTacchio, L., Hayes, K. R., Vollmers, C., Pulivarthy, S., Baggs, J. E., Panda, S., and Hogenesch, J. B. (2009) Harmonics of circadian gene transcription in mammals. *PLoS Genet.* **5,** e1000442

36. Goldberg, I. J., Eckel, R. H., and Abumrad, N. A. (2009) Regulation of fatty acid uptake into tissues: lipoprotein lipase- and CD36-mediated pathways. *J. Lipid Res.* **50** (Suppl), S86–S90

37. Ortega, F. J., Mayas, D., Moreno-Navarrete, J. M., Catalan, V., Gomez-Ambrosi, J., Esteve, E., Rodriguez-Hermosa, J. I., Ruiz, B., Ricart, W., Peral, B., Fruhbeck, G., Tinahones, F. J., and Fernandez-Real, J. M. (2010) The gene expression of the main lipogenic enzymes is downregulated in visceral adipose tissue of obese subjects. *Obesity (Silver Spring)* **18,** 13–20

38. Triqueneaux, G., Thenot, S., Kakizawa, T., Antoch, M. P., Safi, R., Takahashi, J. S., Delaunay, F., and Laudet, V. (2004) The orphan receptor Rev-erbalpha gene is a target of the circadian clock pacemaker. *J. Mol. Endocrinol.* **33,** 585–608

39. Stenbit, A. E., Tsao, T. S., Li, J., Burcelin, R., Geenen, D. L., Factor, S. M., Houseknecht, K., Katz, E. B., and Charron, M. J. (1997) GLUT4 heterozygous knockout mice develop muscle insulin resistance and diabetes. *Nat. Med.* **3,** 1096–1101

40. Pircher, P., Chomez, P., Yu, F., Vennstrom, B., and Larsson, L. (2005) Aberrant expression of myosin isoforms in skeletal muscles from mice lacking the Rev-erbAalpha orphan receptor gene. *Am. J. Physiol.* **288,** R482–490

41. Manttari, S., and Jarvilehto, M. (2005) Comparative analysis of mouse skeletal muscle fibre type composition and contractile responses to calcium channel blocker. *BMC Physiol.* **5,** 4

42. Ibrahimi, A., Bonen, A., Blinn, W. D., Hajri, T., Li, X., Zhong, K., Cameron, R., and Abumrad, N. A. (1999) Muscle-specific overexpression of FAT/CD36 enhances fatty acid oxidation by contracting muscle, reduces plasma triglycerides and fatty acids, and increases plasma glucose and insulin. *J. Biol. Chem.* **274,** 26761–26766

43. Ferraro, R. T., Eckel, R. H., Larson, D. E., Fontvieille, A. M., Rising, R., Jensen, D. R., and Ravussin, E. (1993) Relationship between skeletal muscle lipoprotein lipase activity and 24-hour macronutrient oxidation. *J. Clin. Invest.* **92,** 441–445

44. Tsutsumi, K., Inoue, Y., and Kondo, Y. (2002) The relationship between lipoprotein lipase activity and respiratory quotient of rats in circadian rhythms. *Biol. Pharm. Bull.* **25,** 1360–1363

45. Jensen, D. R., Knaub, L. A., Konhilas, J. P., Leinwand, L. A., MacLean, P. S., and Eckel, R. H. (2008) Increased thermoregulation in cold-exposed transgenic mice overexpressing lipoprotein lipase in skeletal muscle: an avian phenotype? *J. Lipid Res.* **49,** 870–879

46. Schutz, Y. (2004) Concept of fat balance in human obesity revisited with particular reference to de novo lipogenesis. *Int. J. Obes. Relat. Metab. Disord.* **28** (Suppl. 4), S3–S11

47. Raspe, E., Duez, H., Mansen, A., Fontaine, C., Fievet, C., Fruchart, J. C., Vennstrom, B., and Staels, B. (2002) Identifica-

tion of Rev-erbalpha as a physiological repressor of apoC-III gene transcription. *J. Lipid Res.* **43,** 2172–2179

48. Lau, P., Fitzsimmons, R. L., Raichur, S., Wang, S. C., Lechtken, A., and Muscat, G. E. (2008) The orphan nuclear receptor, RORalpha, regulates gene expression that controls lipid metabolism: staggerer (SG/SG) mice are resistant to diet-induced obesity. *J. Biol. Chem.* **283,** 18411–18421

49. Staels, B., and Auwerx, J. (1992) Perturbation of developmental gene expression in rat liver by fibric acid derivatives: lipoprotein lipase and alpha-fetoprotein as models. *Development* **115,** 1035–1043

50. Merkel, M., Weinstock, P. H., Chajek-Shaul, T., Radner, H., Yin, B., Breslow, J. L., and Goldberg, I. J. (1998) Lipoprotein lipase expression exclusively in liver. A mouse model for metabolism in the neonatal period and during cachexia. *J. Clin. Invest.* **102,** 893–901

51. Kim, J. K., Fillmore, J. J., Chen, Y., Yu, C., Moore, I. K., Pypaert, M., Lutz, E. P., Kako, Y., Velez-Carrasco, W., Goldberg, I. J., Breslow, J. L., and Shulman, G. I. (2001) Tissue-specific overexpression of lipoprotein lipase causes tissue-specific insulin resistance. *Proc. Natl. Acad. Sci. U. S. A.* **98,** 7522–7527

52. Voshol, P. J., Jong, M. C., Dahlmans, V. E., Kratky, D., Levak-Frank, S., Zechner, R., Romijn, J. A., and Havekes, L. M. (2001) In muscle-specific lipoprotein lipase-overexpressing mice, muscle triglyceride content is increased without inhibition of insulin-stimulated whole-body and muscle-specific glucose uptake. *Diabetes* **50,** 2585–2590

53. Hensley, L. L., Ranganathan, G., Wagner, E. M., Wells, B. D., Daniel, J. C., Vu, D., Semenkovich, C. F., Zechner, R., and Kern, P. A. (2003) Transgenic mice expressing lipoprotein lipase in adipose tissue. Absence of the proximal 3′-untranslated region causes translational upregulation. *J. Biol. Chem.* **278,** 32702–32709

54. Gonzales, A. M., and Orlando, R. A. (2007) Role of adipocyte-derived lipoprotein lipase in adipocyte hypertrophy. *Nutr. Metab. (Lond.)* **4,** 22

55. Bey, L., Etienne, J., Tse, C., Brault, D., Noe, L., Raisonnier, A., Arnault, F., Hamilton, M. T., and Galibert, F. (1998) Cloning, sequencing and structural analysis of 976 base pairs of the promoter sequence for the rat lipoprotein lipase gene. Comparison with the mouse and human sequences. *Gene* **209,** 31–38

56. Doi, M., Hirayama, J., and Sassone-Corsi, P. (2006) Circadian regulator CLOCK is a histone acetyltransferase. *Cell* **125,** 497–508

57. Nader, N., Chrousos, G. P., and Kino, T. (2009) Circadian rhythm transcription factor CLOCK regulates the transcriptional activity of the glucocorticoid receptor by acetylating its hinge region lysine cluster: potential physiological implications. *FASEB J.* **23,** 1572–1583

58. Gimble, J. M., and Floyd, Z. E. (2009) Fat circadian biology. *J. Appl. Physiol.* **107,** 1629–1637

59. Gachon, F., Leuenberger, N., Claudel, T., Gos, P., Jouffe, C., Fleury Olela, F., de Mollerat du Jeu, X., Wahli, W., and Schibler, U. (2011) Proline- and acidic amino acid-rich basic leucine zipper proteins modulate peroxisome proliferator-activated receptor alpha (PPARalpha) activity. *Proc. Natl. Acad. Sci. U. S. A.* **108,** 4794–4799

60. Schoonjans, K., Peinado-Onsurbe, J., Lefebvre, A. M., Heyman, R. A., Briggs, M., Deeb, S., Staels, B., and Auwerx, J. (1996) PPARalpha and PPARgamma activators direct a distinct tissue-specific transcriptional response via a PPRE in the lipoprotein lipase gene. *EMBO J.* **15,** 5336–5348

61. Andrews, J. L., Zhang, X., McCarthy, J. J., McDearmon, E. L., Hornberger, T. A., Russell, B., Campbell, K. S., Arbogast, S., Reid, M. B., Walker, J. R., Hogenesch, J. B., Takahashi, J. S., and Esser, K. A. (2010) CLOCK and BMAL1 regulate MyoD and are necessary for maintenance of skeletal muscle phenotype and function. *Proc. Natl. Acad. Sci. U. S. A.* **107,** 19090–19095